Cell Reports

Article

A fungal GPI-anchored protein gene functions as a virulence and antiviral factor

Graphical abstract

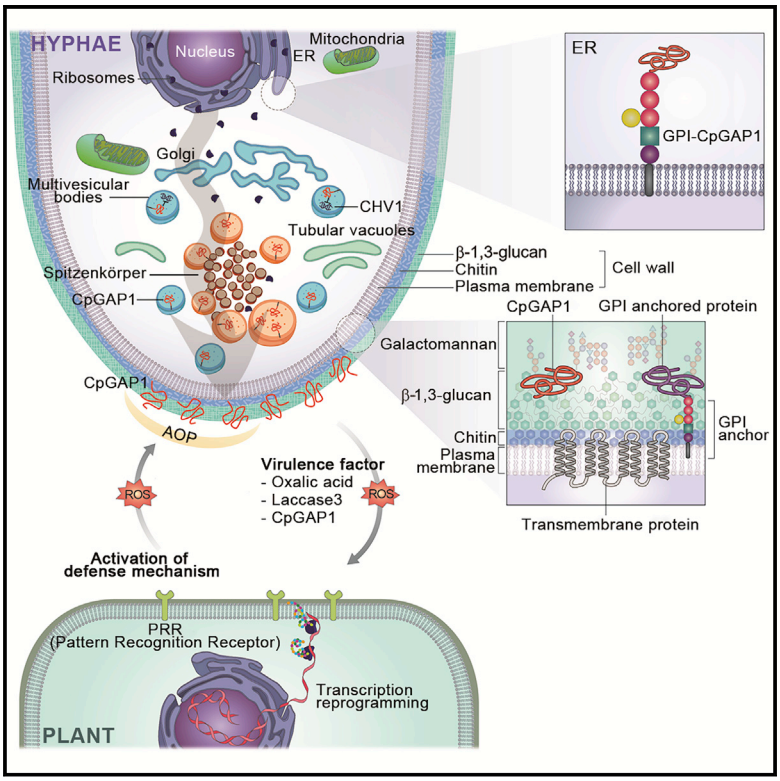

Highlights

- The GPI-AP of *Cryphonectria parasitica* is an antioxidant barrier against host defenses
- The GPI-AP of *C. parasitica* functions as an active phytotoxic factor for pathogenicity
- The GPI-AP is required for tolerance of *C. parasitica* to hypovirus infection
- The GPI-AP of *C. parasitica* functions as an antiviral host factor

Authors

Jeesun Chun, Yo-Han Ko, Kum-Kang So, Su-Hwan Cho, Dae-Hyuk Kim

Correspondence

dhkim@jbnu.ac.kr

In brief

Chun et al. show that a *C. parasitica* GPI-anchored protein (GPI-AP) is essential for virulence and phytotoxicity through an antioxidant activity-dependent mechanism. They furthermore show that GPI-AP functions as an antiviral factor against the mycovirus CHV1.

Chun et al., 2022, Cell Reports *41*, 111481
October 11, 2022
https://doi.org/10.1016/j.celrep.2022.111481

CellPress

Cell Reports

CellPress
OPEN ACCESS

Article

A fungal GPI-anchored protein gene functions as a virulence and antiviral factor

Jeesun Chun,[1,2] Yo-Han Ko,[1,2] Kum-Kang So,[1,2] Su-Hwan Cho,[1] and Dae-Hyuk Kim[1,3,*]

[1]Department of Molecular Biology, Department of Bioactive Material Sciences, Institute for Molecular Biology and Genetics, Jeonbuk National University, Jeonju, Jeonbuk 54896, Korea

[2]These authors contributed equally

[3]Lead contact

*Correspondence: dhkim@jbnu.ac.kr

https://doi.org/10.1016/j.celrep.2022.111481

SUMMARY

We show that a gene (*CpGap1*) encoding a glycosylphosphatidylinositol-anchored protein (GPI-AP) of the chestnut blight fungus *Cryphonectria parasitica* is differentially expressed by Cryphonectria hypovirus 1 (CHV1) infection. Functional analysis using a *CpGap1*-null mutant results in no observed changes in cultural morphology other than hypersensitivity to ROS. Analysis of the protein product of the *CpGap1* gene (CpGAP1) confirmed motifs with antioxidizing properties. The virulence of the *CpGap1*-null mutant is significantly decreased, and phytotoxic activity is seen in the peptides of CpGAP1. CHV1 transfer to the *CpGap1*-null mutant results in severely retarded colonial growth, and virus-titer is significantly increased in the mycelia of CHV1-infected *CpGap1*-null mutant. These results indicate that CpGAP1 functions as a protective barrier against plant defenses, but also acts as a virulence factor. Moreover, our study demonstrates that the *CpGap1* gene is a host-tolerating antiviral factor that helps maintain fungal growth and suppress viral titer after CHV1 infection.

INTRODUCTION

The chestnut blight fungus, *Cryphonectria parasitica* (Murrill) Barr, has eradicated chestnut forests and orchards in North America since the beginning of the 20th century (Van Alfen, 1982). Most interestingly, the infection of the fungal host with a single stranded RNA (ssRNA) mycovirus, Cryphonectria hypovirus 1 (CHV1), attenuates fungal virulence, referred to as hypovirulence, and shows the characteristic symptoms associated with hypovirulence, including reduced pigmentation, sporulation, laccase production, and oxalate accumulation (Anagnostakis, 1982; Nuss, 1992; Van Alfen et al., 1975). Although phenotypic changes in virus-infected strains are pleiotropic, multi-omics studies have indicated that a specific set of fungal genes is affected by the CHV1 infection (Allen et al., 2003; Chen et al., 1996; Chun et al., 2020; Kang et al., 2000; Li et al., 2018a, 2018b). The mitogen-activated protein kinase (MAPK) signaling pathway is one of the most important coordinate regulatory mechanisms associated with numerous virus-mediated fungal genes that regulate viral symptom development (Choi et al., 2005; Deng et al., 2007; Kim et al., 2016; Park et al., 2004, 2012; Sun et al., 2009; Turina et al., 2006).

Recent studies of the MAPK pathway that regulates cell wall integrity (CWI) in *C. parasitica* have revealed that it is specifically regulated by infection with CHV1 (Kim et al., 2016; Moretti et al., 2014; Rostagno et al., 2010; Turina et al., 2006), and that the loss of function mutants of the CWI MAPK pathway showed the characteristic phenotypic changes, including sporadic sectorization (i.e., sporadic occurrence of robust mycelial growth without differentiation) (Kim et al., 2016; So et al., 2017). The sectored area is significantly different from the remaining portion of the parental strain, inasmuch as mycelial growth is recovered but with almost no signs, such as sporulation and pigmentation, of typical differentiation. Moreover, when the mycelia of the sectored area are successively transferred to new media, the progenies of the sectors maintain the characteristics of the sectored phenotypes, indicating that, once sectored, the sectored phenotype is stably inherited. Based on dramatic phenotypic changes of sectors from the parental strain and stable inheritance of sectored phenotype, it has been suggested that the massive changes in the genetics of the sectored progenies had occurred and were maintained. Ultimately, our recent research has shown that global changes in DNA methylation accompanied the sectored progenies (So et al., 2018).

In general terms, CHV1 alters fungal gene expression in a manner that prevents *C. parasitica* from progressing through its normal developmental process. This occurs with near normal vegetative mycelial growth, but a lack of differentiation, as indicated by reduced pigmentation, sporulation, and virulence (Anagnostakis, 1982; Nuss, 1992; Van Alfen et al., 1975). The sectored phenotype, like the viral symptom, shows robust hyphal growth without differentiation. By studying the genes typically involved in CHV1 regulation and the sectored phenotype, we improved our understanding of both viral symptom development and/or fungal virulence, despite the fact that neither of the examined genes is responsible for all of the phenotypic changes.

A recent massive transcript analysis using RNA-sequencing identified specific genes regulated by both sectorization and CHV1 infection (Chun et al., 2019). Among the genes discovered was one encoding for a glycosylphosphatidylinositol (GPI)-anchored protein. GPIs are specific glycolipid anchors that facilitate the attachment of soluble proteins at the outer surface of the plasma membrane and further to the cell wall via *trans*-mannosylation of GPI moiety to the cell wall β-1,6-glucan (Ferguson et al., 2009; Kollár et al., 1997). Proteins are posttranslationally modified in the endoplasmic reticulum (ER) with the GPI anchor to become GPI-anchored proteins (GPI-APs). These are, in turn, inserted into the luminal leaflet of the ER membrane, from whence they follow the secretory pathway to the plasma membrane, where they remain in the external leaflet of the lipid bilayer (Muñiz and Riezman, 2016). The fungal cell wall is pivotal to the maintenance of cellular integrity and for protection against adverse environmental conditions. This dynamic structure continuously changes depending on culture conditions and environmental stresses (Geoghegan et al., 2017; Latgé, 2007). The fungal wall consists of layered reticulate networks carrying glucans, chitin, and embedded proteins such as GPI-APs and proteins with internal repeats. GPI-APs are ubiquitous in eukaryotic organisms and are implicated in diverse biological processes, including ligand recognition, enzymatic activity, cell-to-cell interaction, host infection, and defense triggering (Chang et al., 2018; Li et al., 2018a, 2018b; McConville and Ferguson, 1993; Song et al., 2021). Little is known, however, about the function of fungal GPI-APs beyond their enzymatic activities in cell wall biogenesis. Moreover, although several studies on *C. parasitica* have suggested the importance of cell wall- or membrane-associated proteins for fungal pathogenesis (Gao and Nuss, 1996; Kazmierczak et al., 2005; So and Kim, 2017), neither GPI-anchored nor cell wall proteins have yet been characterized in *C. parasitica*.

In this study, we characterized the biological function of a GPI-AP gene, which is sectorization- and CHV1-specific, and explored the molecular mechanism implicated in fungal virulence and hypovirulence. Our study highlighted the function of a GPI-AP as a virulence factor with antioxidant and phytotoxic properties in a phytopathogenic fungus, as well as its involvement in fungal tolerance as part of the response to CHV1 infection.

RESULTS

Characterization of *CpGap1* gene

Among the 22 identified differentially expressed genes (DEGs) that manifested differences in the accumulation of transcripts by sectorization and hypoviral infection, a DEG tentatively identified as a GPI-AP was selected for further analyses (Chun et al., 2019). The corresponding gene was identified by analyzing the genome sequence of *C. parasitica* (http://genome.jgi-psf.org/Crypa2/Crypa2.home.html). A 4,536-base pair (bp) PCR amplicon containing the full-length genomic GPI-AP fragment was cloned and sequenced. The sequence analyses of the cloned fragment revealed that the determined sequences of the PCR amplicon comprised the sequences of the selected DEG. A near full-length cDNA of the GPI-AP gene was predicted *in silico* and cloned using a pair of primers (CpGap1-cF1 and CpGap1-cR1) at the positions of nucleotide (nt) −3 to 13 and 768 to 781, respectively (1 is the first nucleotide of the start codon). A sequence comparison of the cDNA with the corresponding genomic DNA revealed that the cloned gene consisted of two exons, with an intron at 394 to 486 that was consistent with the prediction of the ORF finder. The nucleotide sequence around the start codon matched Kozak's consensus sequence in which the −3 position was the A in AAACCATG. Rapid amplification of cDNA ends revealed that the 3′-terminus was determined to be T at 256-bp downstream of the stop codon and a putative polyadenylation signal sequence consisting of AATAAA was found 11-bp upstream of the 3′-terminus.

The deduced protein product of the cloned gene consisted of 224 amino acid residues, with an estimated molecular weight of 24.9 kDa and an acidic pI of 5.05 (GenBank: XM_040916577). An analysis of sequence homology using the deduced amino acids revealed that the cloned gene was highly similar to other putatively suggested fungal GPI-APs from *Diaporthe ampelina* (67%), *Fusarium heterosporum* (55%), *Colletotrichum truncatum* (54%), *Ophiostoma piceae* (49%), *Sporothrix insectorum* (48%), *Colletotrichum higginsianum* (48%), *Colletotrichum incanum* (48%), *Rutstroemia* sp. (47%), and *Sporothrix schenckii* (46%). In addition, multiple alignment of nine closely related fungal GPI-APs showing an E value of ∼0.0 and a representative GPI-AP from *Saccharomyces cerevisiae* revealed that the cloned gene had conserved domain structures consisting of an N-terminal signal peptide and a C-terminal GPI-attachment signal region that itself was composed of relatively small amino acids proximal to the GPI-anchored amino acid residue (ω site), as well as terminal hydrophobic residues (Figure S1). However, a domain search of the deduced amino acid sequence using Pfam revealed no additional matches in other fungal GPI-APs, including CFEM (common in fungal extracellular membrane) domain, which is characteristic of eight conserved cysteine residues and unique in fungal proteins (Kulkarni et al., 2006), and the Ser-Thr-rich GPI-anchored family domain (Song et al., 2021). A phylogenetic analysis indicated that the protein product of the cloned gene clustered together with other fungal GPI-APs and the cloned gene with the GPI-AP from *D. ampelina* grouped into a distinct evolutionary lineage with a high bootstrap value suggesting a genuine evolutionary relationship (Figure S2). Taking into account the significant homology to known fungal GPI-APs and the presence of the conserved GPI-attachment signal domains, the cloned gene was referred as *CpGap1*, as it was the first characterized GPI-AP gene of *C. parasitica*.

Expression of *CpGap1*

Since our previous transcriptomic analyses indicated that the accumulation of the *CpGap1* transcripts was affected in the mycelia of CHV1-infected hypovirulent strain UEP1 as compared with those of the wild type (Chun et al., 2019), we examined the accumulation of gene transcripts using the standard liquid culture and real-time quantitative reverse transcription PCR (real-time qRT-PCR) (Figure 1A). Under standard liquid culture conditions, the amount of *CpGap1* transcript in the wild type gradually decreased until 3 days after inoculation, at which point it increased sharply, peaking 7 days after inoculation. In the

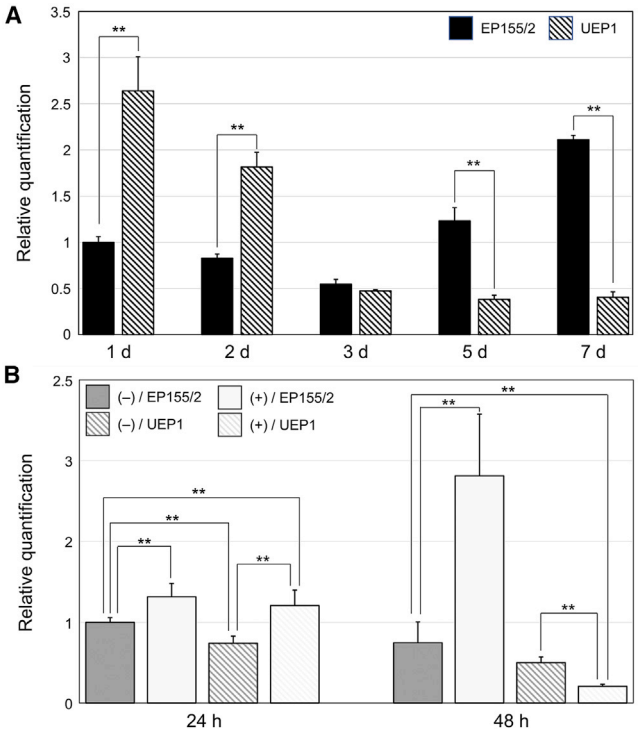

Figure 1. Expression analyses of *CpGap1*

(A) qRT-PCR results of expression levels of *CpGap1* during cultivation in standard liquid EP complete medium and (B) during cultivation on tannic acid (TA)-supplemented medium. Numbers at bottom indicate days (d) and hours (h) in liquid culture and TA-supplemented medium. Strains are indicated on the upper-left, and (+) and (–) indicate media with or without TA supplementation, respectively. Changes in expression of *CpGap1* among strains relative to the level of *gpd* (glyceraldehyde-3-phosphate dehydrogenase) are shown. At least three individual experiments were performed. Error bars represent mean ± SD. Student's t test (n = 3) was used to compare data between two groups, **p < 0.01. Strains used were virus-free wild-type EP155/2 and its isogenic CHV1-infected UEP1 strains.

UEP1 strain, in contrast, the *CpGap1* transcript was significantly upregulated until 2 days after inoculation, at which time it dramatically decreased, although less so than in the virus-free wild type (Figure 1A). These results indicated that *CpGap1* gene expression was tightly regulated by CHV1.

We also examined *CpGap1* gene expression under the solid culture conditions supplemented with tannic acid (TA), a well-known and abundant plant defense component in chestnut trees (Dai and Mumper, 2010). TA supplementation significantly changed the accumulation of *CpGap1* transcripts in both wild-type and CHV1-infected UEP1 strains. The *CpGap1* gene was significantly upregulated at 24 h after growth in TA-supplemented media in the wild type, and further increased at 48 h. CHV1-infected UEP1 strains cultured on the TA-supplemented medium showed a slight but significant upregulation at 24 h but a drastic downregulation at 48 h after the transfer (Figure 1B). These results indicated that *CpGap1* gene expression was also affected by the presence of the host plant's factor such as TA, and that *CpGap1* induction by TA supplementation is significantly disrupted by CHV1.

Construction and identification of the *CpGap1*-null mutant

To examine the biological function of the *CpGap1* gene, a site-directed mutagenesis was attempted by integrative transformation-mediated gene replacement. A total of 95 transformants showing hygromycin B resistance were obtained and screened for the expected gene replacement by PCR using a pair of outer gene-specific primers (Primers P1 & P2 in Figure S3A) corresponding to nt −2,111 to −2,091 and 2,453 to 2,473, relative to the start codons of *CpGap1*. PCR analysis revealed that one transformant showed a 6,991-bp PCR amplicon corresponding to the expected sizes of the replaced alleles of the *CpGap1* gene (data not shown). This PCR amplicon of the putative replaced allele was further confirmed by sequencing. Southern blot analyses of the putative *CpGap1*-null mutant using *Bam*HI digestion and a probe prepared using the 633-bp PCR amplicon containing the 3′-flanking region of the *CpGap1* gene showed a hybridizing band at 1.7 kb. This hybridizing band was different from that of the wild type at 2.4 kb and consistent with the expected size of the *CpGap1*-null mutant allele (Figure S3B). Thus, these results clearly indicate that the selected transformant (termed TdGAP1 for a transformant resulting from deletion of *CpGap1*) had undergone recombination at the *CpGap1* locus, resulting in replacement of the wild-type *CpGap1* gene with the *CpGap1*-null mutant gene.

Morphological and cultural characteristics of the *CpGap1*-null mutant

Colony morphology of the *CpGap1*-null mutant was compared with that of the wild-type EP155/2. No differences in the growth rate, pigmentation, and sporulation were observed on PDAmb under standard growth conditions (constant low-level light at 25°C; Figure 2A).

Responses to environmental changes and abiotic cellular stress

As GPI-AP is important for the maintenance of CWI, we examined the response of the *CpGap1*-null mutant to various external stimuli.

We assessed temperature sensitivity at 20°C and 32°C (cold and hot temperatures) in addition to the control optimum temperature of 25°C (Figure 2A). As the temperature obviated from the optimum, strains showed retarded growth, though no differences in colonial growth and characteristics were observed between the *CpGap1*-null mutant and the wild type, suggesting that the mutation in the *CpGap1* gene had resulted in no changes to temperature sensitivity.

We examined responses to osmotic stress. Supplementation with up to 2.5 $_{M}$ of sorbitol (an osmotic stabilizer) resulted in no observed differences in colony morphology in the *CpGap1*-null mutant (Figure S4).

We also examined the *CpGap1*-null mutant's responses to cell wall-perturbing agents such as Congo red (CR), Calcofluor white (CFW), and SDS. These cell wall-perturbing agents are known to bind to cell wall components and interfere with cell wall composition. As reflected in Figure 2B, no difference between the wild-type EP155/2 and the *CpGap1*-null mutant were observed in response to the CR and CFW. Notably, however, the

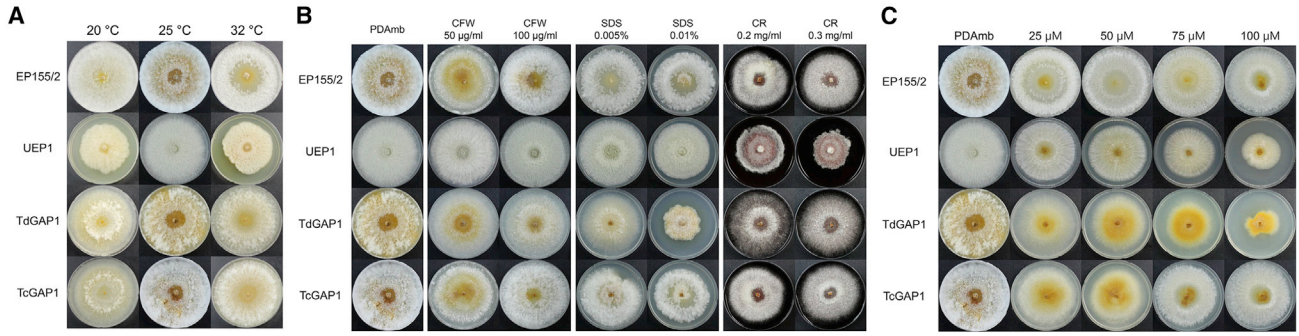

Figure 2. Characteristics of colony morphology of the *CpGap1*-null mutant

(A) Colony morphology of *CpGap1*-null mutant at different temperatures. Colonies are shown after 14 days of cultivation on PDAmb. Temperatures are indicated at the top of the panel. Note that 25°C, 20°C, and 32°C represent the standard optimum, chronic cold, and hot temperatures, respectively.

(B) Colonial morphology of the *CpGap1*-null mutant in response to the cell wall-perturbing agent, CFW, SDS, and CR.

(C) Effect of reactive oxygen species stress on *CpGap1* strain. Concentrations of menadione are indicated at the top of panel. Strains, indicated at left, are the wild-type EP155/2, virus-infected UEP1, *CpGap1*-null mutant (TdGAP1), and complemented strain of TdGAP1 (TcGAP1).

CpGap1-null mutant had more severe growth defects when cultured on plates containing SDS. CR and CFW are known to have a specific binding affinity to chitin, while SDS is a representative anionic surfactant that affects covalently bound cell wall proteins and activates CWI signaling (Schroeder and Ikui, 2019), resulting in alterations to cell wall biosynthesis. A fungal cell wall consists of chitin, glucans, galactomannan, and glycoproteins (Gow et al., 2017). The variations in cell wall impairment (hypersensitivity of the *CpGap1*-null mutant to SDS but not to CR or CFW) suggested that *CpGap1* is involved in CWI as a cell wall-bound protein, and is most likely cross-linked to an outmost glucan but not chitin backbone structure.

We explored responses to reactive oxygen species (ROS) stress. Strains were grown on PDAmb supplemented with appropriate concentrations of menadione and cultural characteristics of the *CpGap1*-null mutant were compared with the wild type. As shown in Figure 2C, the *CpGap1*-null mutant showed aberrant growth above the 50 μ_M menadione level and dramatic retardation of colonial growth at 100 μ_M menadione. The *CpGap1*-null mutant produced more distinctive pigment with drastically decreased aerial hyphae over the compact mycelial. No other mutants, including *CpSlt2* or cryparin (Kazmierczak et al., 2005; So et al., 2017), which present with impaired CWI or cell wall proteins, showed this level of morphological retardation at 100 μ_M menadione, suggesting that the *CpGap1*-null mutant is specifically hypersensitive to ROS. These results indicate that the *CpGap1* gene plays an important role in the response to ROS stress, but via a mechanism that differs from those implicated in CWI (Figure 2C).

To ensure the phenotypic changes attributed to the *CpGap1*-null mutant were due to the mutation in the *CpGap1* gene, we subjected the *CpGap1*-null mutant to complementation via *in trans* transformation with a wild-type *CpGap1* gene. PCR amplification of the wild-type allele of *CpGap1* confirmed that the complemented transformants acquired a wild-type allele of *CpGap1*. The *in trans* complemented strains (designated TcGAP1 for a transformant resulting from complementation of *CpGap1*) recovered the characteristic responses of the wild type to SDS and ROS (Figures 2B and 2C), indicating that the mutant phenotypes were caused by the deletion of the *CpGap1* gene.

Antioxidant property of the protein product of the *CpGap1* gene

Since the *CpGap1*-null mutant showed such dramatic hypersensitivity to the known ROS agent, we checked whether the protein product of the *CpGap1* gene (CpGAP1) had an antioxidant property (AOP) using the database at https://services.healthtech.dtu.dk/service.php?AnOxPePred-1.0. The *in silico* analysis predicted that a CpGAP1 was composed of five peptides with high free radical scavenge scores ($\geq$0.53) (Table S1), implying that there are motifs that possess high free radical scavenging activities. We then synthesized these five peptides and tested for their antioxidant properties.

An ABTS (2,2-azino-bis(3-ethylbenzothiazoline-6-sulfonic acid)) radical scavenging assay based on the generation of an ABTS cation radical chromophore was performed to measure the antioxidant properties of the synthetic peptides (Prior et al., 2005). As shown in Figure 3, all synthetic peptides showed antioxidant properties, though to varying degrees. Among the five synthetic peptides, peptides S1 and S2 showed the least antioxidant activity, equivalent to 0.033 and 0.074 m_M of Trolox (vitamin E analogue), while synthetic peptides S3 and S4 showed the highest activity of 0.481 and 0.405 m_M of Trolox. These results are comparable to those of the well-known antioxidant agent Quercetin. Synthetic peptide S5 showed intermediate levels of activity of 0.275 m_M of Trolox. In sum, two peptides have scavenging activity as good as that of Quercetin, one peptide is lower, and two have little scavenging activity. These results indicated that CpGAP1 is capable of functioning as an antioxidant protein against free radicals and possibly ROS stress generated by host-parasite interactions.

Subcellular localization of the CpGAP1 protein

To determine the CpGAP1 protein's subcellular localization, GFP was used to label. An N-terminal signal peptide suitable for peptidase cleavage at 15 amino acid residue and residue with affinity for a GPI anchor (S192) were predicted for CpGAP1

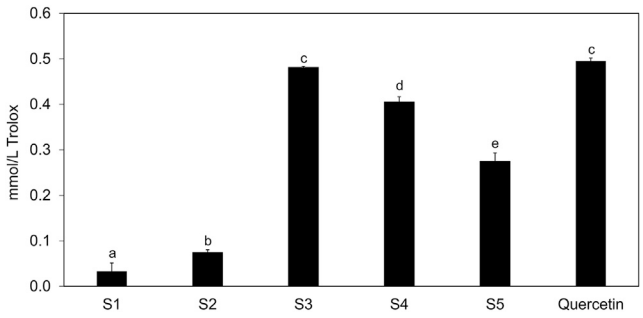

Figure 3. Scavenging capacity (on ABTS^{+}) of peptides of the GPI-anchored protein

The scavenging activity was expressed as Trolox equivalent (mmol/L). Error bars represent SD. Different letters indicate significant differences between samples according to the Duncan test (n = 3) at p = 0.01 using SPSS software (version 18.0, SPSS Inc.).

(Figure S1). The gene encoding GFP (*Gfp*) was thus inserted immediately after the N-terminal signal peptide (GFP:CpGAP1). The GFP-tagged expression cassette was used to transform the *CpGap1*-null mutant, and the resulting transformants were examined to observe the subcellular localization of CpGAP1 using confocal laser scanning microscopy. Compared with the wild type, the fluorescence of GFP:CpGAP1 of selected transformants was distinctive, indicating the expression of these proteins. The fluorescence was also concentrated along the surface of the mycelia and within the intracellular vesicles, indicating cell-surface localization of CpGAP1 delivered by vesicular transport within the secretory pathway (Figure 4). Hypersensitivity of the *CpGap1*-null mutant to ROS was complemented with GFP:CpGAP1 expression, suggesting that the GFP tagging did not disturb the function of CpGAP1 and its subcellular localization.

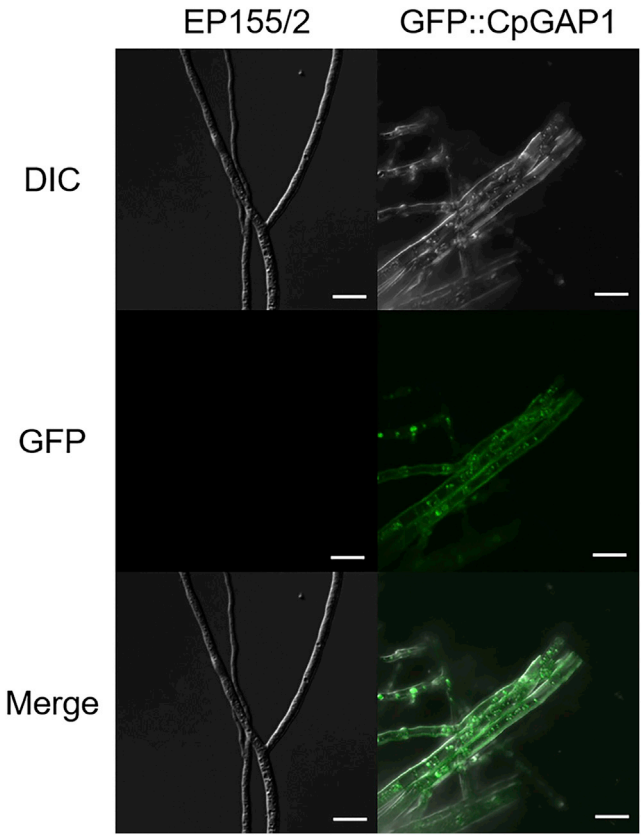

Figure 4. Expression of GFP-tagged CpGAP1 proteins

After 14 days of cultivation on PDAmb, aerial mycelia were placed on a slide glass and analyzed using a confocal laser scanning microscope. Strains are indicated at the top of the panel. Differential interference contrast micrographs, GFP fluorescence micrographs, and merged micrographs are shown from the left to right, respectively, for each strain. Scale bar represents 10 μm.

Virulence assay

We performed a Bavendamm assay, which measures phenoloxidase activity and is known as an indicator of *C. parasitica* virulence. As shown in Figure S5, the area and intensity of the distinctive brown coloration around the colonies, which is an indicator of phenoloxidase activity, was reduced in the *CpGap1*-null mutant compared with the wild-type strain. The size and intensity of the browning area in the *CpGap1*-null mutant was intermediate, falling somewhere between that of the wild-type and the hypovirulent UEP1 strains. These results indicate that the phenoloxidase activity was hampered by *CpGap1* gene mutation.

We examined stroma formation and the active pathogenic growth of the *CpGap1*-null mutant on chestnut tree bark by inoculating mutant strains near to excised stems (Figure 5A). The *CpGap1*-null mutant showed less conspicuous stromal growth and produced fewer stroma than the wild-type and the complemented strain, suggesting a reduced level of pathogenic growth.

We next examined the virulence of the *CpGap1*-null mutant using the excised bark from a chestnut tree. Consistent with the Bavendamm assay and the pathogenic growth results, the size of the necrotic area induced on the excised bark by the *CpGap1*-null mutant was significantly smaller than that induced by the wild-type EP155/2. Moreover, the size of the necrotic area of the *CpGap1*-null mutant was smaller than that of the hypovirulent UEP1 strain (Figure 5B). Recalling that the growth rate of the wild-type and *CpGap1*-null mutant strains was similar, the remarkable reduction in the size of the necrotic area of the *CpGap1*-null mutant suggests the *CpGap1* gene's importance to determine the virulence of *C. parasitica*.

Interestingly, the virulence of the *CpGap1*-null mutant was even lower than that of the hypovirulent strain. We therefore tested whether, in addition to possessing a protective AOP, the CpGAP1 protein might act as an active stressor of plant cells. To test the stress activity by CpGAP1 peptides, we used an *in vitro* experimental system of leaf discs (Kumar et al., 2012; Nol et al., 2012). As shown in Figure 6A, leaf discs floating on the solution at concentrations of 50 μ_M of synthetic peptides did not show significant symptoms within 24 h of treatment. However, depending on the peptide used, leaf discs began to show differences in chlorophyll fluorescence, as measured by the maximum quantum yield of photosystem II (PSII) (F_v/F_m), after extended exposure to some peptide solutions, reflecting the photosynthetic potential in plants under stress (Figure 6A). Peptide S4 showed the second most AOP activity, resulting in a

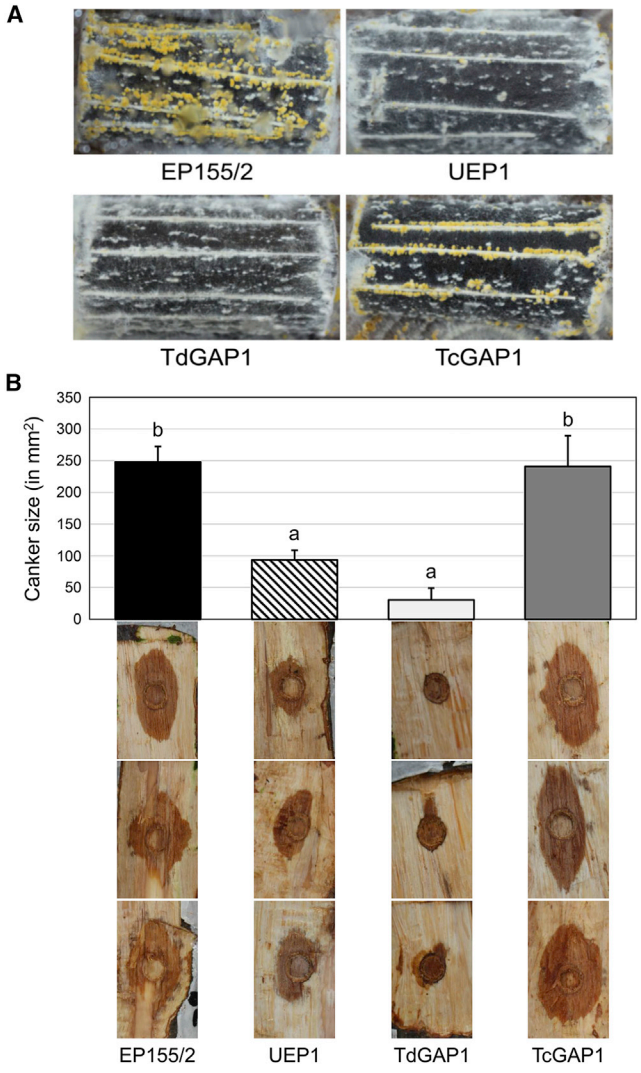

Figure 5. Virulence assays

(A) Pathogenic growth of strains on the stem of the chestnut tree. Stromal pustule eruptions of strains are shown on chestnut tree stems. Note that the number of stromal pustule eruptions of the mutant strain TdGAP1 are dramatically decreased but they are observed on the surface of stem regardless of wound.

(B) Virulence assay using excised chestnut tree bark. Lesion measurement values are shown as SEM (mm^2). Different letters indicate significant differences between treatments according to Duncan's multiple range test (n = 3) at $^{**}p < 0.01$. Error bars represent mean ± SD. A representative figure of excised tree bark 1 week after inoculation is shown below. The strains used are the wild-type EP155/2, virus-infected UEP1, *CpGap1*-null mutant (TdGAP1), and complemented strain of TdGAP1 (TcGAP1).

dramatic decrease in value of PSII (F_v/F_m), reflecting damaged photosynthetic organelles. Others showed no difference from the control solution (Figure 6A). Chlorophyll content measured 5 days after floating was lowest with peptide S4, which was consistent with the order of damaged chlorophyll fluorescence (Figure 6B). According to these results, besides protective antioxidant properties, peptide treatment administered to leaf disc tissue is attended by a peptide-specific response with regard to phytotoxicity. Interestingly, exposure to the same concentration of the mature protein, i.e., a CpGAP1 protein without an N-terminal signal peptide and a C-terminal GPI-anchoring signal, triggered a dramatic decrease in chlorophyll content without conspicuous chlorosis and necrosis, suggesting the existence of additional phytotoxic motifs other than antioxidant peptides.

Effect of hypovirus infection on the colony morphology of the *CpGap1*-null mutant

To examine the biological functions of the *CpGap1* gene in response to hypovirus infection, we analyzed phenotypic changes between virus-free and virus-transmitted isogenic transformants. Following co-culturing of the recipient *CpGap1*-null mutant with UEP1, at least three separated agar blocks containing actively growing mycelia of putatively virus-transmitted sections were independently transferred onto a new hygromycin B-containing PDAmb plate and then single-spored to ensure nuclear homogeneity. The single-spored progenies were tested for the presence of double-stranded RNA (dsRNA) by agarose gel electrophoresis before further comparisons were made. Based on the success of the viral transfer via hyphal fusion to the *CpGap1*-null mutant, we concluded that the loss of function mutation of the *CpGap1* gene did not impair cell-to-cell recognition, i.e., vegetative compatibility, which was represented by hyphal fusion followed by transfer of cytoplasmic CHV1.

When the hypovirus from UEP1 was transferred to the *CpGap1*-null mutant, characteristic phenotypic changes caused by the hypovirus infection (such as reduced pigmentation and asexual sporulation) were observed in the virus-containing *CpGap1*-null mutant. However, compared with the CHV1-infected UEP1 and the CHV1-free *CpGap1*-null mutant, colonial growth of the virus-transmitted *CpGap1*-null mutant was severely retarded (Figure 7A). These phenotypic characteristics were stably maintained during the successive subcultures of the virus-containing *CpGap1*-null mutant. Since retarded growth of the *CpGap1*-null mutant by CHV1 infection suggested that the *CpGap1* gene could play a role in antiviral activity, we measured viral titer in the CHV1-infected *CpGap1*-null mutant to determine whether reduced fungal growth could be ascribed to extensive viral multiplication. Compared to UEP1, a significant increase (more than a 4-fold increase) of the hypovirus titer per gram of mycelia was observed in the retarded colonies of the CHV1-infected *CpGap1*-null mutant (Figures 7B and 7C). To understand the molecular mechanism associated with the increased viral titer, we conducted transcriptional analyses of representative antiviral genes such as the dicer-like *dcl2* and the argonaute-like *agl2* genes in this fungus (Segers et al., 2007). Although the induction of both antiviral genes was observed in the CHV1-infected *CpGap1*-null mutant compared with its CHV1-free counterparts, no significant difference in the accumulation of both *dcl2* and *agl2* transcripts was observed between the CHV1-infected mutant strain and the CHV1-infected wild-type strain (UEP1) (Figure S6). These results suggest that the presence of the *CpGap1* gene is not required as a fungal host factor for the replication of the hypovirus, but that it is required to ensure the physiological tolerance of *C. parasitica* to hypoviral infection and for the suppression of viral replication as an antiviral factor.

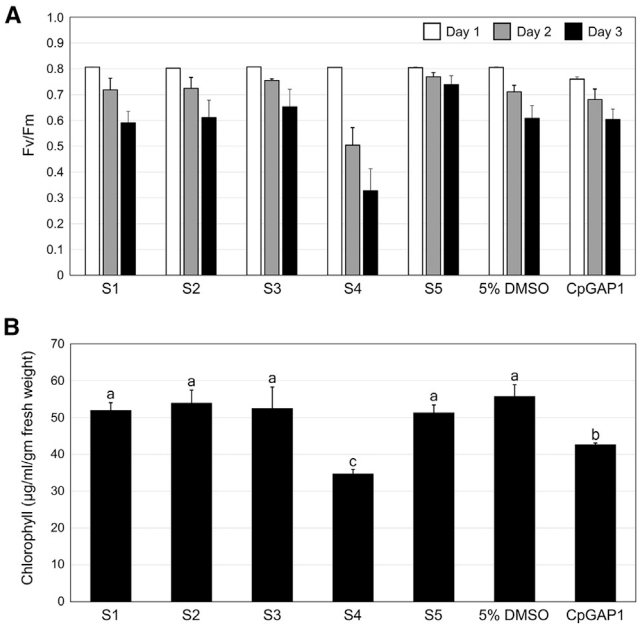

Figure 6. Assessment of phytotoxic activity of synthetic peptides and mature protein of the *CpGap1* gene

(A) Chlorophyll florescence measured as changes in maximum quantum yield of PSII photosystem during a 5-day period. Significant differences were observed only in S4-treated samples after 3 days according to the Duncan test (n = 3) at p = 0.01 using SPSS software (version 18.0, SPSS Inc.).

(B) Total chlorophyll content measured in leaves after 5-day treatment. At least three individual leaf discs were examined. Error bars represent mean ± SD. Different letters indicate significant differences between samples according to the Duncan test (n = 3) at p = 0.01 using SPSS software (version 18.0, SPSS Inc.).

DISCUSSION

The fungal cell wall is dynamic, albeit rigid, and complex structure that maintains cellular integrity and protects the cell from external aggressors. Glucans, chitin, and embedded proteins are major fungal cell wall constituents, among which GPI-APs, covering approximately 1% of protein-encoding genes in eukaryotic genome (Yeats et al., 2018), comprise the majority of the embedded cell wall proteins. GPI-APs, which are ubiquitous in eukaryotes, are diverse in structure and function. Recent studies on the GPI-APs of phytopathogenic fungi, including *Ustilaginoidea virens* and *Aspergillus flavus*, revealed their functions as a proteinaceous microbe-associated molecular pattern (MAMP) that induces immunity in an organ-specific manner and as a virulence factor for host infection and colonization (Chang et al., 2018; Song et al., 2021). Nevertheless, the specific role of the vast majority of GPI-APs play in host-parasite interactions, especially interactions in plant pathogenic fungi, remains largely unknown.

GPI-APs can be classified into two groups according to their subcellular localization, i.e., the plasma membrane protein and cell wall protein. The presence of the stretches of serine upstream the ω-proximal region, which is the marking feature of cell wall protein (De Groot and Brandt, 2012; Frieman and Cormack, 2003), the lack of transmembrane helixes (Bowman and Free, 2006), and the pI value greater than 5 (Pittet and Conzelmann, 2007) suggested that our GPI-AP was a cell wall protein bound covalently to cell wall polysaccharides through the glycan moiety of the GPI. This conclusion is consistent with the responses of the *CpGap1*-null mutant that showed distinct sensitivity to SDS supplementation among three cell-wall-disturbing agents. SDS is known as an agent with weak alkali that has a mild effect, and as suitable for the gentle treatments necessary to harvest fungal cell wall material without perturbing the strong covalent bonds. In contrast, CFW and CR are known to be specific to cell wall chitin and β-glucan, respectively. The more distinctive effect by the SDS strongly suggested that the protein product of the *CpGap1* gene is tightly linked neither to the plasma membrane nor to the core fibrillary structures such as a chitin layer, but rather that it is embedded in the outer cell wall. The absence of the protein product of the *CpGap1* gene appears to affect the cell's surface physical properties. In addition, the hypersensitive reaction in response to the presence of SDS is consistent with that shown in response to ROS, in which hypersensitivity to supplemented menadione was also observed because SDS is also known to generate oxidative stress to the cell (Mizutani et al., 2016).

Mutations in cell wall proteins are likely to result in impairment of CWI; in our case, cell walls spontaneously displayed hypersensitivity to various cell wall stressors, including ROS. However, our mutant strains did not show the hypersensitivity to CR and CFW, but only to ROS. Moreover, the *in silico* analysis indicated that the protein products of the *CpGap1* gene have antioxidant motifs, and the AOP activity of synthetic peptides corresponding to motifs confirmed this. These results indicate that the hypersensitivity to ROS is specific, not general, to characteristics of the *CpGap1* gene.

ROS plays a dual role during host-parasite interactions, and its generation along the plant cell's surface during plant-pathogen interactions is a well-known phenomenon. Plant-generated ROS acts as a direct defense that kills pathogens, or as secondary defense messenger that activates durable host resistance against invading pathogens. Plants accumulate ROS as a significant and earliest pathogen-triggered immune response (Lehmann et al., 2015; Marschall and Tudzynski, 2016; Norvienyeku et al., 2017; Palukaitis and Carr, 2008). In contrast, pathogen-generated ROS that are structurally and functionally similar to the ROS fostered by plants act as virulence factors that damage hosts and suppress host immune systems during host-parasite interactions (Bryan et al., 2012; Heller and Tudzynski, 2011). Successful pathogens are those that have evolved strategies capable of overcoming the host-derived high-ROS environment and that use intracellular ROS as signaling molecules for the development and infection processes (Marschall and Tudzynski, 2016). Elsewhere, the involvement of ROS generators such as H_2O_2 in response to fungal colonization in chestnut trees has been reported (Baptista et al., 2007), which strongly suggests that the bark is able to generate ROS at levels sufficient to act as a strong defense mechanism during pathogen interaction. Necrotrophic pathogens such as *C. parasitica* even depend on the host plant's oxidative burst to achieve its full pathogenicity (Marschall and Tudzynski, 2016). The strong AOP of the amino

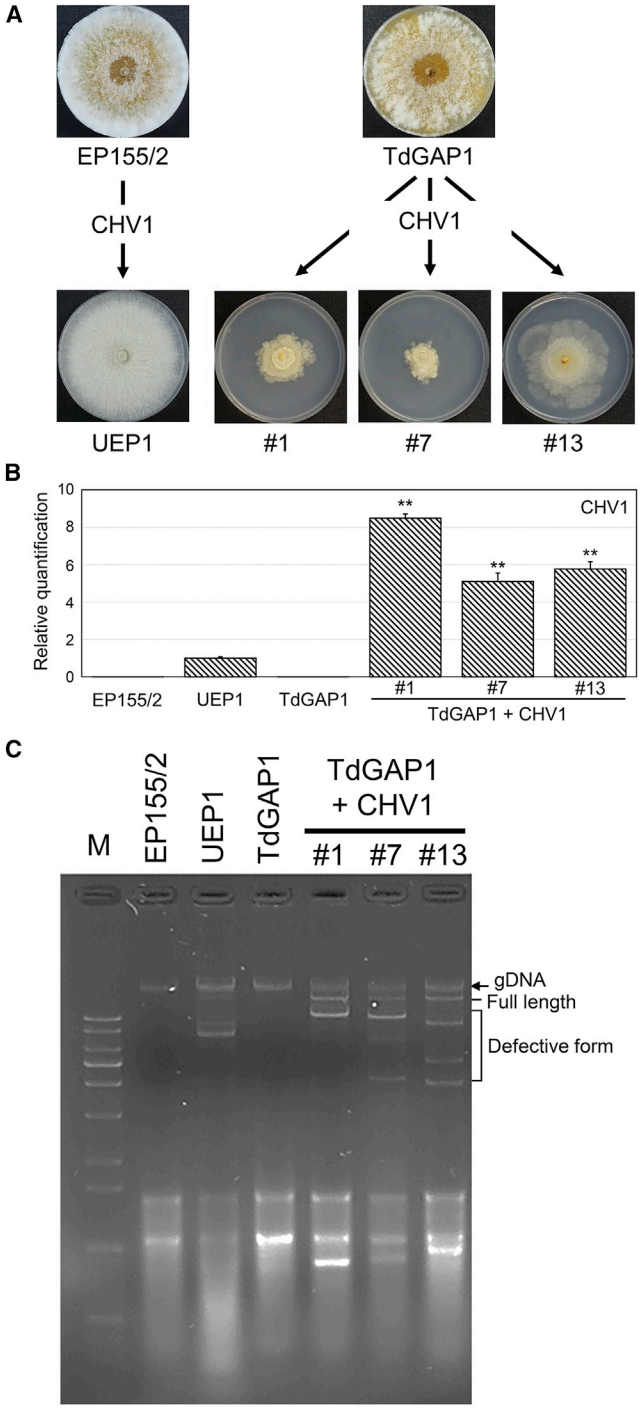

Figure 7. Effect of transferred hypovirus CHV1-713 on the *CpGap1*-null mutant strain

(A) Colony morphology of CHV1-free (upper) and -infected (lower) mutant strains. Virus-free mutant strain (TdGAP1) and its virus-infected isogenic mutant strains (TdGAP1-V^{+}-1, −7, and −13), which were independently obtained, are shown with a control pair consisting of virus-free wild-type (EP155/2) and its virus-infected isogenic strain (UEP1).

(B) qRT-PCR analysis of viral ssRNA accumulation. The levels of ssRNA accumulation of indicated strains are represented as the fold change relative to that of the UEP1. At least three individual experiments were performed. Error bars represent mean ± SD. Student's t test (n = 3) was used to compare data between two groups, **p < 0.01.

(C) Agarose gel electrophoresis of CHV1 preparations. Strains are indicated at the top of the lanes. The positions of fungal genomic DNA, full-length CHV1, and defective viral RNA elements are indicated.

acid composition of the *CpGap1* gene therefore suggests that the anchored protein product of the *CpGap1* gene plays an important role in allowing *C. parasitica* to cope with the high ROS conditions that exist at the fungus-plant interface. It is likely that when *C. parasitica* is initially introduced to the chestnut tree, the plant defense material (possibly tannic acid) is recognized, and a TA-inducible enzyme such as laccase 3 is expressed to degrade the preexisting defense material (Chung et al., 2008). The resulting as well as generating ROS (later with intracellular ROS from necrotic plants) should be tolerated by the cell-surface antioxidizing protein such as the *CpGap1* protein to defend the invading fungal mycelia, then fungal phytotoxic substance such as oxalic acid results in necrosis of plant cells (Chen et al., 2010; Zhang et al., 2013). Accordingly, the strong AOP of the protein product of the *CpGap1* gene and the reduced virulence of the *CpGap1*-null mutant suggest that this gene is a virulence factor. Anti-ROS mechanisms are classified as either enzymatic or non-enzymatic defense systems. Although less is known about non-enzymatic defense systems, which consist of small soluble molecules (including glutathione) that are oxidized to remove oxidants from the solution, genes for the enzymatic defense proteins (including SOD, peroxidase, catalase, and thioredoxin) illustrate the important effect of anti-ROS mechanisms on pathogenicity and survival (Gleason et al., 2014; Heller and Tudzynski, 2011; Liu et al., 2016; Samalova et al., 2014; Wang et al., 2021; Youseff et al., 2012). The significance of other putative anti-ROS mechanisms is less clear, as no functional study has been conducted to date on the non-enzymatic antioxidizing GPI-AP. Our study demonstrated that the *CpGap1*-null mutant became hypersensitive to ROS stress and produced smaller lesions, indicating that the GPI-anchored cell wall protein with its AOP acts as a defense mechanism in response to ROS stress and plays an important role in pathogenicity.

CpGAP1 also functions as a stress factor to plant cells. Leaf disc analysis, which measured chlorophyll fluorescence, was a convenient and non-destructive means of evaluating the level of damage induced by stresses such as osmotic (Chiu et al., 2021), cold (Ehlert and Hincha, 2008; Savitch et al., 2001), high light (Chaerle et al., 2007), wounding (Quilliam et al., 2006), insect (Rodriguez et al., 2014), and pathogen infection (Štambuk et al., 2021). Although the plant tissue used to measure stress activity was not from the original host plant and further studies will be required to understand the molecular mechanism of phytotoxicity, our leaf disc assay was nevertheless capable of assessing stress activity, in as much as we tested the synthetic peptides and protein instead of the pathogen itself. The leaf disc assay confirmed that only a specific antioxidant peptide motif of CpGAP1 contained characteristics that stressed the plant tissues. These results clearly suggest that aside from their role in numerous biological processes, such as filamentation, mating,

flocculation, and adhesion by GPI-cell wall proteins (Hoyer, 2001), our GPI-cell wall protein acted as a protective surface structural barrier to defend the fungus against stress conditions such as ROS, as well as an active factor to induce stress in plant tissues. These defensive and offensive CpGAP1 functions make a significant contribution to fungal pathogenesis.

Severe retardation of colonial growth of the *CpGap1*-null mutant was observed after CHV1 infection. Taking into account the significant increases in the viral titer of the mycelium of the CHV1-infected *CpGap1*-null mutant, the *CpGap1* gene must be directly involved in the antiviral response that inhibits viral replication. Several fungal host factors in *C. parasitica* raise its tolerance for physiological stress induced by a biotic agent, such as CHV1 infection, with or without changes in viral titer (Ko et al., 2021; Lim et al., 2010; Zhang et al., 2006). However, the *CpGap1* protein, which was localized in the cell surface, not intracellular, compartment, has antiviral as well as pro-tolerance functions. Mycoviruses are known to function as a trigger and target of RNA silencing, a representative antiviral response in fungi (Mochama et al., 2018). Our results showed that the absence of the *CpGap1* gene did neither affect the transcriptional induction of both of *dcl2* and *agl2* genes in the RNA silencing complex by CHV1 infection nor reveal significant difference in viral titer between CHV1-infected *CpGap1*-null mutant and its CHV1-free counterpart. These results suggest that antiviral response due to both of these antiviral genes is not related to the *CpGap1* gene. Hypovirus is known to be capsidless and replicates cytoplasmically in fungal host-derived *trans*-Golgi network membranous vesicles. CHV1 infection disturbs the vesicle-mediated secretory pathway of the fungal host and even proliferation of vesicles were observed in CHV1-infected fungal cells. Vesicle formation, trafficking, and occupation are each important for the CHV1 replication and transcription (Jacob-Wilk et al., 2006; Kazmierczak et al., 2012; Shi et al., 2019; Wang et al., 2013). The secretory pathway that includes the ER and vesicles is important for the posttranslational processing of GPI-APs, and the remodeling of the vesicle membrane is a key factor after/for the transglycosylation of GPI moiety to GPI-APs. Therefore, it is highly likely that the absence of the protein product of the *CpGap1* gene affects normal vesicle formation and trafficking, which has implications for CHV1 replication and the fungal secretory pathway. Our results indicate that the expression and localization of the *CpGap1* gene product shares common factors with CHV1 replication, which adopts fungal membranous vesicles and disturbs the fungal secretory pathway. Accordingly, the loss of the function mutant of the *CpGap1* gene results in debilitating the suppression of viral replication for enhanced viral proliferation, which increases the physiological burden on the fungal host, as reflected in the retarded mycelial growth of the CHV1-infected *CpGap1*-null mutant. Therefore, downregulation of the *CpGap1* gene in the hypovirulent UEP1 strain indicates that CHV1 infection downregulates *CpGap1* gene expression in a manner that lessens the antiviral response but supports vegetative hyphal growth.

GPI-APs are known to be involved in membrane enzymes, organizing components, and extracellular matrix adhesins (Chang et al., 2018; Hoyer, 2001). However, little is known of the function of GPI-APs in phytopathogenic fungi. Although the importance of global GPI-anchoring and the required presence of specific GPI-APs for fungal pathogenicity were suggested in *Magnaporthe oryzae* and *Fusarium* spp. (Liu et al., 2020; Michielse et al., 2009; Rittenour and Harris, 2013; Suga et al., 2016), the molecular mechanisms involved in this pathogenicity remained unclear. GPI-AP's function has only recently been characterized for maize infection in *A. flavus* and contrasting functions of MAMP and pathogenicity in *Ustilaginoidea virens* (Chang et al., 2018; Song et al., 2021). The protein product of the *CpGap1* gene is the first GPI-AP of *C. parasitica* investigated to date. Our study of the GPI-AP clearly demonstrates the molecular mechanism of the phytopathogenic fungal GPI-AP as a virulence factor. In addition, the function of the cell wall anchored protein that is encoded by the *CpGap1* gene has implications for our understanding of the interactions between the intracellular CHV1 and surface-displayed fungal protein via intracellular membranous interactions during biosynthesis of the protein product of the *CpGap1* gene.

Limitations of the study

Although we demonstrate the molecular mechanism that renders the *CpGap1* gene essential for the virulence, as it overcomes host defense mechanism (such as ROS) by non-enzymatic antioxidant activity of its peptide sequences and possesses the phytotoxic activity of resulting peptides to plant cell, there are still several limitations in this work. We used tobacco leaves to measure phytotoxic activity but the establishment of measuring phytotoxicity with an original host plant will greatly reinforce the precise molecular mechanism of fungal virulence. We explain how the spatially distinct cell-surface protein and intracellular mycovirus cross-reacted, inhibited intracellular viral replication, and enhanced fungal tolerance against viral infection. The precise molecular mechanism of posttranslational processing of the protein product of *CpGap1* gene and shared intracellular vesicle trafficking should be further studied to understand the implication of fungus-virus interactions.

STAR★METHODS

Detailed methods are provided in the online version of this paper and include the following:

- KEY RESOURCES TABLE
- RESOURCE AVAILABILITY
  - Lead contact
  - Materials availability
  - Data and code availability
- EXPERIMENTAL MODELS AND SUBJECT DETAILS
  - Fungal strains and culture conditions
- METHOD DETAILS
  - Cloning of CpGap1 and construction of gene knockout strain
  - Quantitative analyses of transcript accumulation by real-time RT-PCR
  - Phenotypic characterization to various stress
  - Antioxidant assay
  - Confocal laser scanning microscopy and fluorescent dyes

- Virulence assays
- Leaf disc assay
- Transmission of dsRNA virus
- Isolation and measurement of viral dsRNA

● QUANTIFICATION AND STATISTICAL ANALYSIS

SUPPLEMENTAL INFORMATION

Supplemental information can be found online at https://doi.org/10.1016/j.celrep.2022.111481.

ACKNOWLEDGMENTS

This work was supported by the National Research Foundation of Korea (NRF) grants by MSIP (2018R1A2A1A05078682 and 2022R1A2C3005906). This research was also supported by Basic Science Research Program through the NRF funded by the Ministry of Education (2017R1A6A1A03015876). We thank the Institute of Molecular Biology and Genetics at Jeonbuk National University for kindly providing the facilities for this research.

AUTHOR CONTRIBUTIONS

J.C., Y.H.K., and K.K.S. contributed equally to this work. J.C. and D.H.K. designed the experiments and analyzed data. S.H.C. identified the mutant. Y.H.K. prepared the figures and analyzed the mutant characteristics. K.K.S. analyzed the antioxidant property and phytotoxicity. D.H.K. supervised the experiments and wrote the manuscript. All authors read and approved the final manuscript.

DECLARATION OF INTERESTS

The authors declare no competing interests.

Received: January 20, 2022
Revised: June 14, 2022
Accepted: September 19, 2022
Published: October 11, 2022

REFERENCES

Allen, T.D., Dawe, A.L., and Nuss, D.L. (2003). Use of cDNA microarrays to monitor transcriptional responses of the chestnut blight fungus *Cryphonectria parasitica* to infection by virulence-attenuating hypoviruses. Eukaryot. Cell *2*, 1253–1265.

Anagnostakis, S.L. (1982). Biological control of chestnut blight. Science *215*, 466–471.

Baptista, P., Martins, A., Pais, M.S., Tavares, R.M., and Lino-Neto, T. (2007). Involvement of reactive oxygen species during early stages of ectomycorrhiza establishment between Castanea sativa and Pisolithus tinctorius. Mycorrhiza *17*, 185–193.

Bowman, S.M., and Free, S.J. (2006). The structure and synthesis of the fungal cell wall. Bioessays *28*, 799–808.

Bryan, N., Ahswin, H., Smart, N., Bayon, Y., Wohlert, S., and Hunt, J.A. (2012). Reactive oxygen species (ROS) - a family of fate deciding molecules pivotal in constructive inflammation and wound healing. Eur. Cell. Mater. *24*, 249–265.

Chaerle, L., Hagenbeek, D., De Bruyne, E., and Van Der Straeten, D. (2007). Chlorophyll fluorescence imaging for disease-resistance screening of sugar beet. Plant Cell Tissue Organ Cult. *91*, 97–106.

Chang, P.-K., Zhang, Q., Scharfenstein, L., Mack, B., Yoshimi, A., Miyazawa, K., and Abe, K. (2018). *Aspergillus flavus* GPI-anchored protein-encoding ecm33 has a role in growth, development, aflatoxin biosynthesis, and maize infection. Appl. Microbiol. Biotechnol. *102*, 5209–5220.

Chen, B., Gao, S., Choi, G.H., and Nuss, D.L. (1996). Extensive alteration of fungal gene transcript accumulation and elevation of G-protein-regulated cAMP levels by a virulence-attenuating hypovirus. Proc. Natl. Acad. Sci. USA *93*, 7996–8000.

Chen, C., Sun, Q., Narayanan, B., Nuss, D.L., and Herzberg, O. (2010). Structure of oxalacetate acetylhydrolase, a virulence factor of the chestnut blight fungus. J. Biol. Chem. *285*, 26685–26696.

Chiu, Y.-C., Chen, B.-J., Su, Y.-S., Huang, W.-D., and Chen, C.-C. (2021). A leaf disc assay for evaluating the response of tea (*Camellia sinensis*) to PEG-induced osmotic stress and protective effects of azoxystrobin against drought. Plants *10*, 546.

Choi, E.S., Chung, H.J., Kim, M.J., Park, S.M., Cha, B.J., Yang, M.S., and Kim, D.H. (2005). Characterization of the ERK homologue CpMK2 from the chestnut blight fungus *Cryphonectria parasitica*. Microbiology *151*, 1349–1358.

Chun, J., Ko, Y.H., and Kim, D.H. (2020). Transcriptome analysis of *Cryphonectria parasitica* infected with Cryphonectria hypovirus 1 (CHV1) reveals distinct genes related to fungal metabolites, virulence, antiviral RNA-silencing, and their regulation. Front. Microbiol. *11*, 1711.

Chun, J., So, K.K., Ko, Y.H., Kim, J.M., and Kim, D.H. (2019). Comparative transcriptomic analysis of MAPK-mediated regulation of sectorization in *Cryphonectria parasitica*. Mol. Cells *42*, 363–375.

Chung, H.J., Kwon, B.R., Kim, J.M., Park, S.M., Park, J.K., Cha, B.J., Yang, M.S., and Kim, D.H. (2008). A tannic acid-inducible and hypoviral-regulated Laccase3 contributes to the virulence of the chestnut blight fungus Cryphonectria parasitica. Mol. Plant Microbe Interact. *21*, 1582–1590.

Cortesi, P., McCulloch, C.E., Song, H., Lin, H., and Milgroom, M.G. (2001). Genetic control of horizontal virus transmission in the chestnut blight fungus, *Cryphonectria parasitica*. Genetics *159*, 107–118.

Dai, J., and Mumper, R.J. (2010). Plant phenolics: extraction, analysis and their antioxidant and anticancer properties. Molecules *15*, 7313–7352.

de Groot, P.W.J., and Brandt, B.W. (2012). ProFASTA: a pipeline web server for fungal protein scanning with integration of cell surface prediction software. Fungal Genet. Biol. *49*, 173–179.

Deng, F., Allen, T.D., Hillman, B.I., and Nuss, D.L. (2007). Comparative analysis of alterations in host phenotype and transcript accumulation following hypovirus and mycoreovirus infections of the chestnut blight fungus *Cryphonectria parasitica*. Eukaryot. Cell *6*, 1286–1298.

Ehlert, B., and Hincha, D.K. (2008). Chlorophyll fluorescence imaging accurately quantifies freezing damage and cold acclimation responses in Arabidopsis leaves. Plant Methods *4*, 12.

Ferguson, M.A.J., Kinoshita, T., and Hart, G.W. (2009). Glycosylphosphatidylinositol anchors. In Essentials of Glycobiology, A. Varki, R.D. Cummings, J.D. Esko, H.H. Freeze, P. Stanley, C.R. Bertozzi, G.W. Hart, and M.E. Etzler, eds. (Cold Spring Harbor Laboratory Press). Ch. 11.

Frieman, M.B., and Cormack, B.P. (2003). The omega-site sequence of glycosylphosphatidylinositol-anchored proteins in *Saccharomyces cerevisiae* can determine distribution between the membrane and the cell wall. Mol. Microbiol. *50*, 883–896.

Gao, S., and Nuss, D.L. (1996). Distinct roles for two G protein alpha subunits in fungal virulence, morphology, and reproduction revealed by targeted gene disruption. Proc. Natl. Acad. Sci. USA *93*, 14122–14127.

Geoghegan, I., Steinberg, G., and Gurr, S. (2017). The role of the fungal cell wall in the infection of plants. Trends Microbiol. *25*, 957–967.

Gleason, J.E., Galaleldeen, A., Peterson, R.L., Taylor, A.B., Holloway, S.P., Waninger-Saroni, J., Cormack, B.P., Cabelli, D.E., Hart, P.J., and Culotta, V.C. (2014). Candida albicans SOD5 represents the prototype of an unprecedented class of Cu-only superoxide dismutases required for pathogen defense. Proc. Natl. Acad. Sci. USA *111*, 5866–5871.

Gow, N.A.R., Latgé, J.P., and Munro, C.A. (2017). The fungal cell wall: structure, biosynthesis, and function. Microbiol. Spectr. *5*, 1.

Heller, J., and Tudzynski, P. (2011). Reactive oxygen species in phytopathogenic fungi: signaling, development, and disease. Annu. Rev. Phytopathol. *49*, 369–390.

Hoyer, L.L. (2001). The ALS gene family of *Candida albicans*. Trends Microbiol. *9*, 176–180.

Jacob-Wilk, D., Turina, M., and Van Alfen, N.K. (2006). Mycovirus Cryphonectria hypovirus 1 elements cofractionate with trans-Golgi network membranes of the fungal host *Cryphonectria parasitica*. J. Virol. *80*, 6588–6596.

Kang, H.S., Choi, J.W., Park, S.M., Cha, B.J., Yang, M.S., and Kim, D.H. (2000). Ordered differential display from *Cryphonectria parasitica*. Plant Pathol. J. *16*, 142–146.

Kazmierczak, P., Kim, D.H., Turina, M., and Van Alfen, N.K. (2005). A hydrophobin of the chestnut blight fungus, *Cryphonectria parasitica*, is required for stromal pustule eruption. Eukaryot. Cell *4*, 931–936.

Kazmierczak, P., McCabe, P., Turina, M., Jacob-Wilk, D., and Van Alfen, N.K. (2012). The mycovirus CHV1 disrupts secretion of a developmentally regulated protein in *Cryphonectria parasitica*. J. Virol. *86*, 6067–6074.

Kim, J.M., Lee, J.G., Yun, S.H., So, K.K., Ko, Y.H., Kim, Y.H., Park, S.M., and Kim, D.H. (2016). A mutant of the *Bck1* homolog from *Cryphonectria parasitica* resulted in sectorization with an impaired pathogenicity. Mol. Plant Microbe Interact. *29*, 268–276.

Kim, J.M., Park, J.A., and Kim, D.H. (2012). Comparative proteomic analysis of chestnut blight fungus, *Cryphonectria parasitica*, under tannic-acid-inducing and hypovirus-regulating conditions. Can. J. Microbiol. *58*, 863–871.

Kim, D.H., Rigling, D., Zhang, L., and Van Alfen, N.K. (1995). A new extracellular laccase of *Cryphonectria parasitica* is revealed by deletion of *Lac1*. Mol. Plant Microbe Interact. *8*, 259–266.

Ko, Y.H., So, K.K., Chun, J., and Kim, D.H. (2021). Distinct roles of two DNA methyltransferases from *Cryphonectria parasitica* in fungal virulence, responses to hypovirus infection, and viral clearance. mBio *12*. e02890-20.

Kollár, R., Reinhold, B.B., Petráková, E., Yeh, H.J., Ashwell, G., Drgonová, J., Kapteyn, J.C., Klis, F.M., and Cabib, E. (1997). Architecture of the yeast cell wall. β (1→6)-glucan interconnects mannoprotein, β (1→3)-glucan, and chitin. J. Biol. Chem. *272*, 17762–17775.

Kulkarni, R.D., Kelkar, H.S., and Dean, R.A. (2006). An eight-cysteine-containing CFEM domain unique to a group of fungal membrane proteins. Trends Biochem. Sci. *28*, 118–121.

Kumar, G., Kushwaha, H.R., Panjabi-Sabharwal, V., Kumari, S., Joshi, R., Karan, R., Mittal, S., Pareek, S.L.S., and Pareek, A. (2012). Clustered metallothionein genes are co-regulated in rice and ectopic expression of OsMT1e-P confers multiple abiotic stress tolerance in tobacco via ROS scavenging. BMC Plant Biol. *12*, 107.

Latgé, J.P. (2007). The cell wall: a carbohydrate armour for the fungal cell. Mol. Microbiol. *66*, 279–290.

Lee, J.K., Tattar, T.A., Berman, P.M., and Mount, M.S. (1992). A rapid method for testing the virulence of *Cryphonectria parasitica* using excised bark and wood of American chestnut. Phytopathology *82*, 1454–1456.

Lehmann, S., Serrano, M., L'Haridon, F., Tjamos, S.E., and Metraux, J.P. (2015). Reactive oxygen species and plant resistance to fungal pathogens. Phytochemistry *112*, 54–62.

Li, R., Bai, S., He, Y., Chen, Q., Yao, Y., Wang, J., and Chen, B. (2019). Cpvma1, a vacuolar H 1-ATPase catalytic subunit of *Cryphonectria parasitica*, is essential for virulence and hypovirus RNA accumulation. Phytopathology *109*, 1417–1424.

Li, J., Mouyna, I., Henry, C., Moyrand, F., Malosse, C., Chamot-Rooke, J., Janbon, G., Latgé, J.P., and Fontaine, T. (2018a). Glycosylphosphatidylinositol anchors from galactomannan and GPI-anchored protein are synthesized by distinct pathways in *Aspergillus fumigatus*. J. Fungi *4*, 19.

Li, R., Zhou, S., Li, Y., Shen, X., Wang, Z., and Chen, B. (2018b). Comparative methylome analysis reveals perturbation of host epigenome in chestnut blight fungus by a hypovirus. Front. Microbiol. *9*, 1026.

Lim, J.G., Lee, J.G., Kim, J.M., Park, J.A., Park, S.M., Yang, M.S., and Kim, D.H. (2010). A DnaJ-like homolog from *Cryphonectria parasitica* is not responsive to hypoviral infection but is important for fungal growth in both wild-type and hypovirulent strains. Mol. Cells *30*, 235–243.

Liu, J., Guan, T., Zheng, P., Chen, L., Yang, Y., Huai, B., Li, D., Chang, Q., Huang, L., and Kang, Z. (2016). An extracellular Zn-only superoxide dismutase from *Puccinia striiformis* confers enhanced resistance to host-derived oxidative stress. Environ. Microbiol. *18*, 4118–4135.

Liu, C., Xing, J., Cai, X., Hendy, A., He, W., Yang, J., Huang, J., Peng, Y.L., Ryder, L., and Chen, X.L. (2020). GPI7-mediated glycosylphosphatidylinositol anchoring regulates appressorial penetration and immune evasion during infection of *Magnaporthe oryzae*. Environ. Microbiol. *22*, 2581–2595.

Livak, K.J., and Schmittgen, T.D. (2001). Analysis of relative gene expression data using real-time quantitative PCR and the $2^{-\Delta\Delta}C^{T}$ method. Methods *25*, 402–408.

Marschall, R., and Tudzynski, P. (2016). Reactive oxygen species in development and infection processes. Semin. Cell Dev. Biol. *57*, 138–146.

McConville, M.J., and Ferguson, M.A. (1993). The structure, biosynthesis and function of glycosylated phosphatidylinositols in the parasitic protozoa and higher eukaryotes. Biochem. J. *294*, 305–324.

Michielse, C.B., van Wijk, R., Reijnen, L., Cornelissen, B.J.C., and Rep, M. (2009). Insight into the molecular requirements for pathogenicity of *Fusarium oxysporum* f. sp. *lycopersici* through large-scale insertional mutagenesis. Genome Biol. *10*, R4.

Mizutani, T., Sumida, H., Sagawa, Y., Okano, Y., and Masaki, H. (2016). Carbonylated proteins exposed to UVA and to blue light generate reactive oxygen species through a type I photosensitizing reaction. J. Dermatol. Sci. *84*, 314–321.

Mochama, P., Jadhav, P., Neupane, A., and Lee Marzano, S.Y. (2018). Mycoviruses as triggers and targets of RNA silencing in white mold fungus *Sclerotinia sclerotiorum*. Viruses *10*, 214.

Moretti, M., Rossi, M., Ciuffo, M., and Turina, M. (2014). Functional characterization of the three mitogen-activated protein kinase kinases (MAP2Ks) present in the *Cryphonectria parasitica* genome reveals the necessity of Cpkk1 and Cpkk2, but not Cpkk3, for pathogenesis on chestnut (*Castanea* spp.). Mol. Plant Pathol. *15*, 500–512.

Muñiz, M., and Riezman, H. (2016). Trafficking of glycosylphosphatidylinositol anchored proteins from the endoplasmic reticulum to the cell surface. J. Lipid Res. *57*, 352–360.

Nguyen, Q.B., Kadotani, N., Kasahara, S., Tosa, Y., Mayama, S., and Nakayashiki, H. (2008). Systematic functional analysis of calcium signalling proteins in the genome of the riceblast fungus, *Magnaporthe oryzae*, using a high-throughput RNA-silencing system. Mol. Microbiol. *68*, 1348–1365.

Nol, N., Tsikou, D., Eid, M., Livieratos, I.C., and Giannopolitis, C.N. (2012). Shikimate leaf disc assay for early detection of glyphosate resistance in *Conyza canadensis* and relative transcript levels of EPSPS and ABC transporter genes. Weed Res. *52*, 233–241.

Norvienyeku, J., Zhong, Z., Lin, L., Dang, X., Chen, M., Lin, X., Zhang, H., Anjago, W.M., Lin, L., Abdul, W., and Wang, Z. (2017). Methylmalonate-semialdehyde dehydrogenase mediated metabolite homeostasis essentially regulate conidiation, polarized germination and pathogenesis in *Magnaporthe oryzae*. Environ. Microbiol. *19*, 4256–4277.

Nuss, D.L. (1992). Biological control of chestnut blight: an example of virus-mediated attenuation of fungal pathogenesis. Microbiol. Rev. *56*, 561–576.

Palukaitis, P., and Carr, J.P. (2008). Plant resistance responses to viruses. J. Plant Pathol. *90*, 153–171.

Park, S.M., Choi, E.S., Kim, M.J., Cha, B.J., Yang, M.S., and Kim, D.H. (2004). Characterization of HOG1 homologue, CpMK1, from *Cryphonectria parasitica* and evidence for hypovirus-mediated perturbation of its phosphorylation in response to hypertonic stress. Mol. Microbiol. *51*, 1267–1277.

Park, J.A., Kim, J.M., Park, S.M., and Kim, D.H. (2012). Characterization of *CpSte11*, a MAPKKK gene of *Cryphonectria parasitica*, and initial evidence of its involvement in the pheromone response pathway. Mol. Plant Pathol. *13*, 240–250.

Pittet, M., and Conzelmann, A. (2007). Biosynthesis and function of GPI proteins in the yeast *Saccharomyces cerevisiae*. Biochim. Biophys. Acta *1771*, 405–420.

Powell, W.A., and Van Alfen, N.K. (1987). Differential accumulation of poly(A)+ RNA between virulent and double-stranded RNA-induced hypovirulent strains of *Cryphonectria (Endothia) parasitica*. Mol. Cell Biol. *7*, 3688–3693.

Prior, R.L., Wu, X., and Schaich, K. (2005). Standardized methods for the determination of antioxidant capacity and phenolics in foods and dietary supplements. J. Agric. Food Chem. *53*, 4290–4302.

Quilliam, R.S., Swarbrick, P.J., Scholes, J.D., and Rolfe, S.A. (2006). Imaging photosynthesis in wounded leaves of *Arabidopsis thaliana*. J. Exp. Bot. *57*, 55–69.

Rittenour, W.R., and Harris, S.D. (2013). Glycosylphosphatidylinositol-anchored proteins in *Fusarium graminearum*: inventory, variability, and virulence. PLoS One *8*, e81603.

Rodriguez, P.A., Hogenhout, S.A., and Bos, J.I.B. (2014). Leaf-disc assay based on transient over-expression in *Nicotiana benthamiana* to allow functional screening of candidate effectors from aphids. Methods Mol. Biol. *1127*, 137–143.

Rolli, E., Ragni, E., Calderon, J., Porello, S., Fascio, U., and Popolo, L. (2009). Immobilization of the glycosylphosphatidylinositol-anchored Gas1 protein into the chitin ring and septum is required for proper morphogenesis in yeast. Mol. Biol. Cell *20*, 4856–4870.

Rostagno, L., Crivelli, G., and Turina, M. (2010). Study of mRNA expression by real time PCR of Cpkk1, Cpkk2 and Cpkk3, three MEKs of *Cryphonectria parasitica*, in virus-free and virus-infected isogenic isolates. J. Phytopathol. *158*, 409–416.

Samalova, M., Meyer, A.J., Gurr, S.J., and Fricker, M.D. (2014). Robust anti-oxidant defences in the rice blast fungus *Magnaporthe oryzae* confer tolerance to the host oxidative burst. New Phytol. *201*, 556–573.

Savitch, L.V., Barker-Astrom, J., Ivanov, A.G., Hurry, V., Oquist, G., Huner, N.P., and Gardeström, P. (2001). Cold acclimation of *Arabidopsis thaliana* results in incomplete recovery of photosynthetic capacity, associated with an increased reduction of the chloroplast stroma. Planta *214*, 295–303.

Schroeder, L., and Ikui, A.E. (2019). Tryptophan confers resistance to SDS-associated cell membrane stress in *Saccharomyces cerevisiae*. PLoS One *14*, e0199484.

Segers, G.C., and Nuss, D.L. (2003). Constitutively activated Gα negatively regulates virulence, reproduction and hydrophobin gene expression in the chestnut blight fungus *Cryphonectria parasitica*. Fungal Genet. Biol. *38*, 198–208.

Segers, G.C., Zhang, X., Deng, F., Sun, Q., and Nuss, D.L. (2007). Evidence that RNA silencing functions as an antiviral defense mechanism in fungi. Proc. Natl. Acad. Sci. USA *104*, 12902–12906.

Shi, L., Wang, J., Quan, R., Yang, F., Shang, J., and Chen, B. (2019). CpATG8, a homolog of yeast autophagy protein ATG8, is required for pathogenesis and hypovirus accumulation in the chest blight fungus. Front. Cell. Infect. Microbiol. *9*, 222.

So, K.K., and Kim, D.H. (2017). Role of MAPK signaling pathways in regulating the hydrophobin cryparin in the chestnut blight fungus *Cryphonectria parasitica*. Mycobiology *45*, 362–369.

So, K.K., Ko, Y.H., Chun, J., Bal, J., Jeon, J., Kim, J.M., Choi, J., Lee, Y.H., Huh, J.H., and Kim, D.H. (2018). Global DNA methylation in the chestnut blight fungus *Cryphonectria parasitica* and genome-wide changes in DNA methylation accompanied with sectorization. Front. Plant Sci. *9*, 103.

So, K.K., Ko, Y.H., Chun, J., Kim, J.M., and Kim, D.H. (2017). Mutation of the *Slt2* ortholog from *Cryphonectria parasitica* results in abnormal cell wall integrity and sectorization with impaired pathogenicity. Sci. Rep. *7*, 9038.

Song, T., Zhang, Y., Zhang, Q., Zhang, X., Shen, D., Yu, J., Yu, M., Pan, X., Cao, H., Yong, M., et al. (2021). The N-terminus of an *Ustilaginoidea virens* Ser-Thr-rich glycosylphosphatidylinositol-anchored protein elicits plant immunity as a MAMP. Nat. Commun. *12*, 2451.

Štambuk, P., Šikuten, I., Preiner, D., Nimac, A., Lazarević, B., Marković, Z., Maletić, E., Kontić, J.K., and Tomaz, I. (2021). Screening of Croatian native grapevine varieties for susceptibility to *Plasmopara viticola* using leaf disc bioassay, chlorophyll fluorescence, and multispectral imaging. Plants *10*, 661.

Suga, H., Kageyama, K., Shimizu, M., and Hyakumachi, M. (2016). A natural mutation involving both pathogenicity and perithecium formation in the *Fusarium graminearum* species complex. G3 *6*, 3883–3892.

Sun, Q., Choi, G.H., and Nuss, D.L. (2009). Hypovirus-responsive transcription factor gene *pro1* of the chestnut blight fungus *Cryphonectria parasitica* is required for female fertility, asexual spore development, and stable maintenance of hypovirus infection. Eukaryot. Cell *8*, 262–270.

Turina, M., Zhang, L., and Van Alfen, N.K. (2006). Effect of Cryphonectria hypovirus 1 (CHV1) infection on Cpkk1, a mitogen-activated protein kinase kinase of the filamentous fungus *Cryphonectria parasitica*. Fungal Genet. Biol. *43*, 764–774.

Van Alfen, N.K. (1982). Biology and potential for disease control of hypovirulence of *Endothia parasitica*. Annu. Rev. Phytopathol. *20*, 349–362.

Van Alfen, N.K., Jaynes, R.A., Anagnostakis, S.L., and Day, P.R. (1975). Chestnut blight: biological control by transmissible hypovirulence in. Science *189*, 890–891.

Wang, Q., Pokhrel, A., and Coleman, J.J. (2021). The extracellular superoxide dismutase Sod5 from *Fusarium oxysporum* is localized in response to external stimuli and contributes to fungal pathogenicity. Front. Plant Sci. *12*, 608861.

Wang, J., Wang, F., Feng, Y., Mi, K., Chen, Q., Shang, J., and Chen, B. (2013). Comparative vesicle proteomics reveals selective regulation of protein expression in chestnut blight fungus by a hypovirus. J. Proteomics *78*, 2221–2230.

Yeats, T.H., Bacic, A., and Johnson, K.L. (2018). Plant glycosylphosphatidylinositol anchored proteins at the plasma membrane-cell wall nexus. J. Integr. Plant Biol. *60*, 649–669.

Youseff, B.H., Holbrook, E.D., Smolnycki, K.A., and Rappleye, C.A. (2012). Extracellular superoxide dismutase protects *Histoplasma* yeast cells from host-derived oxidative stress. PLoS Pathog. *8*, e1002713.

Yu, J.H., Hamari, Z., Han, K.H., Seo, J.A., Reyes-Domínguez, Y., and Scazzocchio, C. (2004). Double-Joint PCR: a PCR-based molecular tool for gene manipulations in filamentous fungi. Fungal Genet. Biol. *41*, 973–981.

Zhang, B., Oakes, A.D., Newhouse, A.E., Baier, K.M., Maynard, C.A., and Powell, W.A. (2013). A threshold level of oxalate oxidase transgene expression reduces *Cryphonectria parasitica*-induced necrosis in a transgenic American chestnut (*Castanea dentata*) leaf bioassay. Transgenic Res. *22*, 973–982.

Zhang, X., Segers, G.C., Sun, Q., Deng, F., and Nuss, D.L. (2006). Characterization of hypovirus-derived small RNAs generated in the chestnut blight fungus by an inducible DCL-2-dependent pathway. J. Virol. *82*, 2613–2619.

STAR★METHODS

KEY RESOURCES TABLE

REAGENT or RESOURCE	SOURCE	IDENTIFIER
Bacterial and virus strains		
Escherichia coli DH5α competent cell	RBC	Cat# RH617
Chemicals, peptides, and recombinant proteins		
Polyethylene glycol 4000	Duchefa Biochemie	Cat# P0804
SDS	Sigma-Aldrich	Cat# 11667289001
Calcoflour White Stain	Sigma-Aldrich	Cat# 18909
Congo Red	Sigma-Aldrich	Cat# C6767
Menadione	Sigma-Aldrich	Cat# M5625
DMSO	Sigma-Aldrich	Cat# D8418
Tannic acid	Sigma-Aldrich	Cat# 403040
CF11	Whatman	Cat# 4021-050
Critical commercial assays		
SYBR green mixture RT kit	Applied Biosystems	Cat# 4344463
Antioxidant assay kit	Sigma-Aldrich	Cat# CS0790
Experimental models: Organisms/strains		
EP155/2	ATCC	Cat# ATCC 38755
UEP1	Powell and Van Alfen (1987)	N/A
CpGap1 knock-out mutant	This paper	N/A
Complemented *CpGap1* knock-out mutant strain	This paper	N/A
Oligonucleotides		
Primers for qRT-PCR analysis, see Table S1	This paper	N/A
Primers for construction of knock-out mutant, see Table S1	This paper	N/A
Recombinant DNA		
GFP::CpGAP1	This paper	N/A
Software and algorithms		
SPSS ver18.0	IBM	https://www.ibm.com/products/spss-statistics
Clustal X2	Clustal	www.clustal.org
MEGA 7	MEGA	www.megasoftware.net
Adobe Photoshop	Adobe	www.adobe.com/products/photoshop.html
Microsoft Excel	Microsoft Office	www.microsoft.com/en-us/microsoft-365/excel

RESOURCE AVAILABILITY

Lead contact

Further information and requests for resources and reagents should be directed to and will be fulfilled by the lead contact, Dae-Hyuk Kim (dhkim@jbnu.ac.kr).

Materials availability

This study did not generate new unique reagents.

Data and code availability

All data reported in this paper will be shared by the lead contact upon request.
This paper does not report original code.
Any additional information required to reanalyze the data reported in this paper is available from the lead contact upon request.

EXPERIMENTAL MODELS AND SUBJECT DETAILS

Fungal strains and culture conditions

C. parasitica strain EP155/2 (ATCC 38755) and its isogenic CHV1-713 containing hypovirulent strain UEP1 were the fungal strains used. The strains were maintained on potato dextrose agar supplemented with L-methionine (0.1 g/L) and biotin (1 mg/L) (PDAmb) and incubated at 25°C under constant low light. Preparation of the primary inoculum for liquid cultures and culture conditions were described previously. Tannic acid (TA) supplementation was also performed as described previously (Kim et al., 1995).

METHOD DETAILS

Cloning of CpGap1 and construction of gene knock-out strain

To obtain and amplify a full-length *CpGap1* cDNA clone, a PCR using reverse transcriptase (RT-PCR) was performed with primers CpGap1-cF1 and CpGap1-cR1. The resulting 675-bp cDNA amplicon was cloned and sequenced. The *CpGap1* knock-out mutant strain was constructed using a double-joint PCR strategy (Yu et al., 2004). The deletion construct (the coding region of *CpGap1* was replaced by a hygromycin B phosphotransferase (*hph*) selection marker with DNA fragments that contained 5′-flanking and 3′-flanking regions of the ORF) was transformed into wild-type strain EP155/2. PEG-mediated protoplast transformation was performed as described elsewhere (Kim et al., 1995, 2012). Gene replacement was confirmed by PCR and Southern blot analysis. In order to complement the *CpGap1* knock-out mutant strain, near full-length genomic DNA of *CpGap1* gene was amplified using PCR and cloned into the vector that contained the geneticin resistance cassette (*G418*) (Nguyen et al., 2008). The resulting vector was used to transform the *CpGap1* knock-out mutant strain. In addition, to label the CpGAP1 protein, the *Gfp* gene encoding the enhanced green fluorescent protein (GFP) (GenBank AYV99744.1) was fused to the *CpGap1* gene immediately after N-terminal signal peptide using PCR (Rolli et al., 2009). The constitutive strong promoter (p188) of the cryparin gene was arranged to express the GFP-fused gene constructs. The resulting constructs were then ligated to the vector containing the geneticin resistance cassette and used to transform the *CpGap1* knock-out mutant strain. Primers used in this study are listed in Table S2.

Quantitative analyses of transcript accumulation by real-time RT-PCR

Real-time PCR was performed using a GeneAmp 7500 sequence detection system (Applied Biosystems) and an SYBR green mixture RT kit (Applied Biosystems) as previously described (Kim et al., 2012). Gene transcript levels were quantified by the $2^{-\Delta\Delta}C^{T}$ method (Livak and Schmittgen, 2001), using glyceraldehyde-3-phosphate dehydrogenase (*gpd*) as the endogenously expressed gene. Accumulation of transcripts of an interest in the wild type and hypovirulent UEP1 strains, with or without TA supplementation, was analyzed by the two-tailed Student's t-test. A p-value of ≤ 0.05 was considered to be significant. Primers used in this study are listed in Table S2.

Phenotypic characterization to various stress

The susceptibility of the null-mutant strain and wild type strain to cell wall perturbing agent was assayed according to the previously described protocol (So et al., 2017). Briefly, each strain was incubated onto a PDAmb agar plate supplemented with either 0.005 to 0.01% SDS, 50 to 100 μg/mL Calcofluor White, or 0.2 to 0.3 mg/mL Congo Red. Fungal growth was analyzed after incubation at 25°C for 14 d. Response to oxidative stress was inspected by monitoring growth of the strains on a PDAmb plate treated with 25–500 μ_M menadione (Segers and Nuss, 2003).

Antioxidant assay

Synthetic peptides were artificially produced through Peptron peptide synthesis using a PeptrEX (Peptron Inc., Daejeon, Korea). Total antioxidant capacity was determined from 30.0 nmole of peptide samples using an antioxidant assay kit (Sigma-Aldrich) according to the instructions provided. Reactions were carried out in a 96-well plate and endpoint absorbance was read at 405 nm using a plate reader (Thermo Scientific, Multiskan GO). Antioxidant concentration was quantified using a Trolox™ standard curve.

Confocal laser scanning microscopy and fluorescent dyes

For imaging, mycelia were arranged on a slide glass, covered with a coverslip, and analyzed in an inverted Olympus FluoviewTM FV1000 confocal microscope fitted with an Argon laser (GFP: excitation, 488 nm; emission, 505-525 nm) and a diode pump solid-state (DPSS, Melles Griot, Carlsbad, CA) laser (mCherry or RFP: excitation, 543 nm; emission, 560-660 nm). Either a 60× Plan Apo N (Olympus) oil-immersion objective (NA, 1.42) or a 40× UPLNF (Olympus) oil-immersion objective (NA, 1.3) were used. Confocal images were captured and examined using FV31S-SW software (version 2.6, Olympus) and further processed with Adobe Photoshop CS5.

Virulence assays

To test the pathogenicity of the strains by measuring phenol oxidase activity, the strains were cultured on Bavendamm's medium supplemented with 0.5% tannic acid. A virulence assay using excised chestnut bark (*Castanea crenata*) were performed as described previously (Lee et al., 1992). After two weeks, the length and width of the cankers were measured.

Leaf disc assay

The tobacco plant *Nicotiana tabacum* L. cv *Xanthi* was used in this study. A cork borer was used to punch out 15 mm diameter leaf discs from 5 to 6 healthy, fully extended, similarly-aged tobacco plant leaves. A total of nine leaf discs were uniformly placed in a covered petri plate (60 mm diameter) containing 6 mL of treatment solution. Synthetic peptides were dissolved in 5% DMSO and 50 μM of each peptide was applied as a treatment solution. The petri plates were sealed and maintained at 24°C for five days. Chlorophyll fluorescence was measured in the center portion of each leaf disc using a CropReporter™ (PhenoVation B.V. Wageningen, the Netherlands). Treated leaf discs were dark-adapted for 30 min prior to measurements. Saturating light and actinic light intensities were set to 3700 and 185 mmolem-2s-1 of PAR, respectively. Chlorophyll fluorescence F_v/F_m which reflects the maximum quantum efficiency of photosystem II was determined as described previously (Chiu et al., 2021). The amount of chlorophyll was assessed using the nine leaf discs using the processes as described previously (Chiu et al., 2021). Concentrations of Chlorophyll a and Chlorophyll b in the sample solution were determined using a spectrophotometer at 663.6 and 646.6 nm, respectively. Total Chlorophyll was estimated by calculating the sum of Chlorophyll a and Chlorophyll b.

Transmission of dsRNA virus

Virus transmission was performed as previously described (Cortesi et al., 2001). Briefly, agar plugs with mycelium of the virus-containing strain UEP1 were inoculated on the other side, adjacent to the mycelial plugs of virus-free recipient transformants on PDAmb. The plates were incubated for seven days to allow mycelia to fuse at the border between each pair of strains. The mycelial plugs were then sampled and inoculated on hygromycin-containing PDAmb. Transmission of virus was confirmed visually by observing phenotypes, such as reduced growth or pigmentation. Virus preservation was also confirmed by successive transfer to hygromycin-containing PDAmb. The putative single-spored virus-infected transformants were selected and tested for the presence of hypovirus by purification of dsRNA.

Isolation and measurement of viral dsRNA

For dsRNA extraction, the UEP1 and dsRNA-transmitted transformants were cultured on PDAmb plates covered with a cellophane membrane over 5 days at 25°C. The 0.2 g wet weight mycelia were collected and ground in liquid nitrogen, and dsRNA was isolated with extraction buffer (2 × STE [0.2 $_M$ NaCl, 0.1 $_M$ Tris- HCl, pH 8.0, 2 m_M EDTA], 2% SDS, 1% sodium bisulfate). dsRNA was purified with two successive rounds of phenol extraction and subsequent treatment of CF11 resin. Viral accumulation was conducted as described in a previous study (Li et al., 2019). Analysis was performed using at least two independent RNA preparations and in triplicate for viral replication using *gpd* as the endogenous control. Primers used in this study are listed in Table S2.

QUANTIFICATION AND STATISTICAL ANALYSIS

All data were analyzed by Student's *t*-test for comparison of two groups or one-way ANOVA combined with Duncan's *post hoc* test for multiple comparisons using SPSS software (version 18.0, SPSS Inc.). The number of experimental replications is represented as n and indicated in the figure legends. All data including error bars are presented as mean ± SD. p-values < 0.01 were considered statistically significant, reported as $^{**}p < 0.01$ in the figure legend.